Semiconductors, 2023, Vol. 57, No. 3

High sensitivity of halide vapor phase epitaxy grown indium oxide films to ammonia

© D.A. Almaev[1], A.V. Almaev[1,2], V.I. Nikolaev[3,4], P.N. Butenko[1,3], M.P. Scheglov[3], A.V. Chikiryaka[3], A.I. Pechnikov[3]

[1] Tomsk State University,
634050 Tomsk, Russia
[2] Fokon LLC,
248009 Kaluga, Russia
[3] Ioffe Institute,
194021 St. Petersburg, Russia
[4] Perfect Crystals LLC,
194223 St. Petersburg, Russia
E-mail: almaev001@mail.ru

Received March 14, 2023
Revised April 13, 2023
Accepted April 13, 2023

The effect of H_2, NH_3, CO and O_2 on the electrically conductive properties of In_2O_3 films grown by halide vapor phase epitaxy has been studied. In the temperature range of $200-550^\circ$C, In_2O_3 films demonstrate gas sensitivity to all considered gases, a relatively high operation speed and repeatability of cycles. The greatest response to NH_3 was obtained, which exceeded 33 arb. units at a temperature of 400°C and a gas concentration of 1000 ppm^{-1}. A qualitative mechanism of gas sensitivity of In_2O_3 films is proposed. The obtained gas-sensitive characteristics are compared with known In_2O_3 sensors based on various materials. It is shown that the method of halide vapor phase epitaxy makes it possible to obtain indium oxide films with high gas sensitivity.

Keywords: In_2O_3 films, halide vapor phase epitaxy, gas-sensitive properties, response.

DOI: 10.21883/SC.2023.03.56229.4704

1. Introduction

Indium oxide — n-type metal oxide semiconductor, which due to optical transparency in the visible area of the spectrum (band gap $E_g = 3.5-3.7$ eV [1–5]), low effective mass of electrons ($m_n = 0.16-0.25$ m [3,6,7]), high catalytic activity and conductivity, caused by the presence of doubly ionized oxygen vacancies, is widely used and can be used in gas sensors, solar cells, touch and liquid crystal displays, thin film transistors, optoelectronic and photovoltaic devices, contacts and Schottky diodes [1–5,8–18]. Such extensive and diverse fields of application are more often attributed to $In_2O_3:Sn$ [1,3,5,8], while the properties of undoped In_2O_3 are most actively studied for gas sensors [1,2,11–18]. In_2O_3 has polymorphism and three main polymorphous modifications are distinguished: body-centered cubic c-In_2O_3; rhombohedral rh-In_2O_3 and orthorhombic o-In_2O_3. c-In_2O_3 is the only thermostable polymorph that attracts the most research interest [1,3,5,8,9,11–16,19–21].

Table 1 lists the gas sensitive properties of structures based on In_2O_3, which demonstrate a high response (S) to various gases at relatively low temperatures (T) and gas concentrations (n_g). It follows from the presented data that In_2O_3 is attractive as gas sensors for NO_2, O_3, ethanol, NH_3 and acetone. Structures based on In_2O_3 demonstrate high sensitivity to NO_2 and O_3 at $n_g < 1$ ppm^{-1} [10,12,14]. Exposure to ethanol and acetone does not always lead to high values S, but studies of sensitivity to these gases are more often found in the literature [2,13,15,16]. The sensors NH_3 based on hierarchical structures In_2O_3 should be specially mentioned, since the gas sensitive characteristics of rh-In_2O_3 are superior to WO_3, which is the most common material for detecting NH_3 [11].

A detailed study of the gas sensitive properties of In_2O_3 is limited due to the lack of high-quality crystals of this material. There is information in the literature [3,4,17–19] on the following methods for growing In_2O_3 films: atomic layer deposition (ALD), pulsed laser deposition (PLD), molecular beam epitaxy (MBE), metal-organic chemical vapor deposition (MOCVD), RF magnetron sputtering (RFMS), electron beam evaporation (EBE), mist-chemical vapor deposition (mist-CVD), low pressure chemical vapor deposition (LPCVD). The method of hydride vapor phase epitaxy (HVPE) is quite new to obtain In_2O_3. By now, there is no much information [17–21] on the growth of In_2O_3 films by the HVPE method, and there is no detailed information on the properties of the obtained crystals. It is known that HVPE is an inexpensive method that allows to achieve very high growth rates, and in some cases it allows to obtain a developed surface, which is especially important in the case of gas sensors [22]. In addition, there are a large number of papers on the production of films of metal oxide semiconductors (MOS) [3,19–28] of high structural quality by the HVPE method.

This paper is devoted to the study of the gas sensitive properties of c-In_2O_3 films obtained by the HVPE method.

Table 1. Gas sensitive properties of structures based on In_2O_3

Material	Acquiring method	T, °C	Gas/n_g	S, arb. units	Source
Films c-In_2O_3	Sol-gel	300	NO_2/100 ppm^{-1}	31.3	[1]
Thin films c-In_2O_3	Spray pyrolysis	370	H_2/3000 ppm^{-1}	25	[10]
		270	O_3/1 ppm^{-1}	2000	
Nanowires c-In_2O_3	Chemical vapor deposition	300	Ethanol/80 ppm^{-1}	1.46	[2]
Hierarchical structures c-In_2O_3	Powder annealing InOOH	300	NH_3/5 ppm^{-1}	17	[11]
Films c-In_2O_3	Sol-gel	350	CO/1000 ppm^{-1}	1.14	[12]
		250	NO_2/900 ppb^{-1}	1.7	
Nanostructures c-In_2O_3	Hydrothermal	90	O_3/100 ppb^{-1}	7.5	[14]
Films c-In_2O_3	Sol-gel	400	Ethanol/5 ppm^{-1}	4	[15]
Microcolours c-In_2O_3	Hydrothermal	220	Acetone/50 ppm^{-1}	4.1	[16]
Hierarchical structures rh-In_2O_3	Powder annealing InOOH	300	NH_3/5 ppm^{-1}	1.9	[11]
Films rh-In_2O_3	Sol-gel	350	CO/1000 ppm^{-1}	1.17	[12]
		250	NO_2/900 ppb^{-1}	1.5	
Nanocolours rh-In_2O_3	Powder Annealing InOOH	280	Ethanol/50 ppm^{-1}	22	[13]
Nanostructures rh-In_2O_3	Hydrothermal	90	O_3/100 ppb^{-1}	12	[14]
Nanostructures $c + rh$-In_2O_3				5.5	
Nanowires $c + rh$-In_2O_3	Sol-gel	300	Ethanol/5 ppm^{-1}	40	[15]
Microcolours $c + rh$-In_2O_3	Hydrothermal	250	Acetone/50 ppm^{-1}	12	[16]

2. Experiment procedure

Films In_2O_3 0.5 μm thick were grown by the HVPE method using gaseous indium chloride and oxygen as precursors. Growth took place on sapphire substrates with basic orientation (0001) 430 μm thick at $T = 600^\circ$C. Special doping of the films was not carried out. Plane-parallel contacts were formed on the surface of the films through a mask by magnetron sputtering of a Pt target with an interelectrode distance of 150 μm.

The phase composition of the samples was studied by X-ray diffraction analysis (XRD), using a diffractometer with an CuK_α-radiation source ($\lambda = 1.5406$ Å) in the $\theta - 2\theta$ scanning mode. The microrelief of the film surface was studied by field effect scanning electron microscopy (FESEM) using an Apreo 2 setup at an accelerating voltage of 2 kV.

Before measuring the gas sensitive characteristics of the films, they were preheated to $T = 550^\circ$C in a clean dry air flow to stabilize the properties of the contacts and regenerate the surface. The gas sensitivity studies were carried out using a Nextron microprobe setup and a Keithley 2636A source-meter. The measurement process was automated using programs developed in the Lab View environment. The measurements were carried out in dark conditions, in a flow of clean dry air or in a gas mixture of clean dry air+target gas. H_2, NH_3, CO and O_2 were chosen as target gases. To exclude the influence of sample history on the results of the experiment, each sample was exposed to only one gas. The flow rate of gas mixtures through the measuring chamber was maintained at a constant level and amounted to 1000 cm^3/min. In the study of the sensitivity of films to oxygen, an $N_2 + O_2$ mixture was used, and the gas mixture flow rate was 500 cm^3/min. The flow of the target gas in the mixture with air was set with an accuracy of $\pm 0.5\%$ using a gas mixture generator Microgas F-06. Gas sensitive characteristics were measured in a wide range T from 30 to 550°C at a constant bias $U = 2$ V.

3. Results and discussion

3.1. Structural properties of films In_2O_3

Analysis of the XRD spectrum of the films In_2O_3 (Fig. 1, *a*) on a logarithmic scale showed the presence of peaks at $2\theta = 30.6$ and 35.5°, corresponding to reflections from the (222) and (004) planes c-In_2O_3. In addition, the X-ray diffraction pattern contains high-intensity reflections from the sapphire substrate, corresponding to the (0001) plane family. The FESEM image (Fig. 1, *b*) shows that

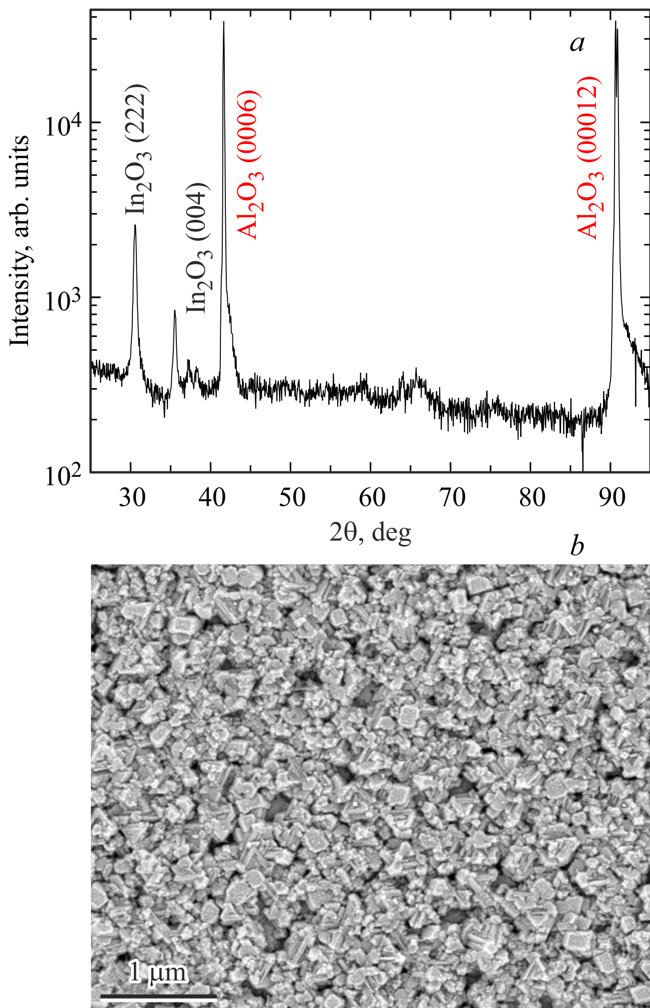

Figure 1. XRD spectrum (a) and FESEM (b) of In_2O_3 films on a sapphire substrate.

the In_2O_3 films have a granular structure with a faceting close to a square shape and a characteristic grain size $D_g = 100-200$ nm.

3.2. Gas-sensing properties of films In_2O_3

The impact of the target gases led to a reversible change in the resistance (R), for the reducing gases H_2, NH_3 and CO the values R decreased, and for O_2 — increased. In this case, the following ratios were chosen to determine the response values S:

$$S_{\text{r.g.}} = R_{\text{air}}/R_g, \quad (1)$$

$$S_{\text{o.g.}} = R_{\text{O}}/R_{\text{N}}, \quad (2)$$

where $S_{\text{r.g.}}$ — response to reducing gases; S_{O} — response to O_2; R_{air}, $R_{\text{r.g.}}$, R_{O} and R_{N} — quasi-stationary values of sample resistances in clean dry air, on exposure to reducing gases, on exposure to O_2 and in the atmosphere N_2, respectively. To evaluate the performance of In_2O_3 films, an analysis of the time dependences of R was carried out and the values of the time constant (t_{res}) and recovery time (t_{rec}) were determined. As t_{res} on exposure to H_2, NH_3 and CO, we took the time interval between the beginning of the action of the corresponding gas mixture on the film and the moment when its resistance is set at the $1.1R_{\text{r.g.}}$ level, and on exposure to O_2 — the time interval between the start of the action of the $N_2 + O_2$ mixture on the film and the establishment of its resistance at the level $0.9R_{\text{O}}$. As t_{rec}, on exposure toH_2, NH_3 and CO, the time interval between the start of blowing through the chamber with clean air samples and the establishment of their resistance at the level of $0.9R_{\text{air}}$ was chosen, and on exposure to O_2 — the time interval between blowing N_2 through the chamber and setting the resistance of the films In_2O_3 at level $1.1R_{\text{N}}$.

The temperature dependences of the response (Fig. 2, a) show that the In_2O_3 films begin to feel CO only at $T \geq 200$°C, for other gases this temperature is higher

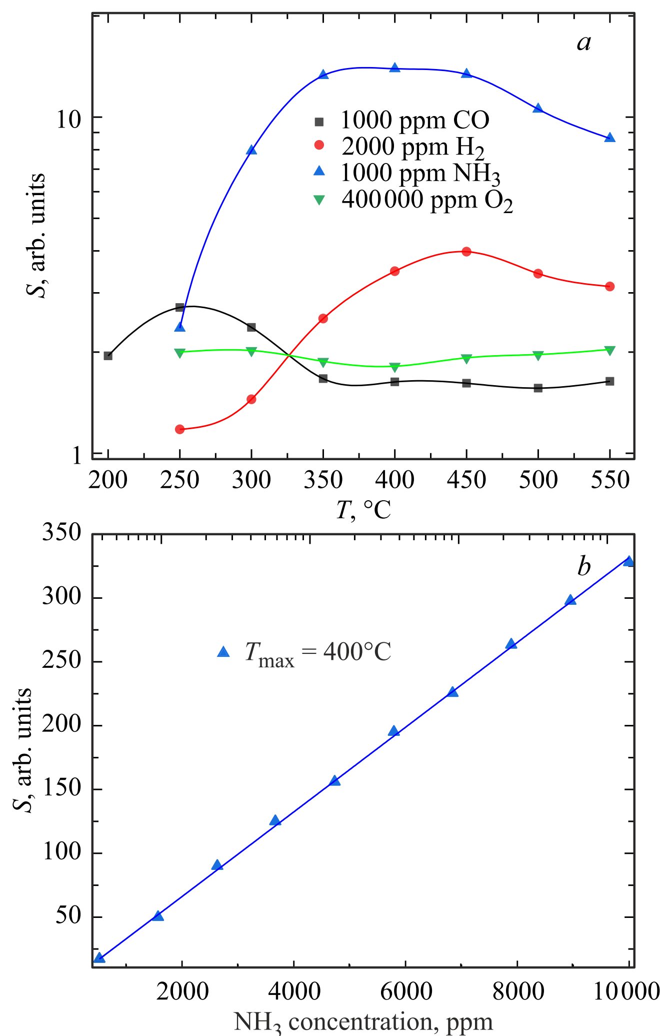

Figure 2. Temperature (a) and concentration (b) dependences of the film response In_2O_3 on exposure to target gases and NH_3, respectively.

Table 2. Values obtained from the analysis of the concentration dependences of the response of In_2O_3 films exposed to CO, H_2 and O_2

Gas	CO		H_2		O_2	
T_{max}, °C	300		450		550	
n_g, ppm^{-1}	600	10^4	580	10^4	$4 \cdot 10^4$	10^6
S, arb. units	1.7	3.3	4.1	9.5	1.3	4.2

by 50°C. The $S(T)$ curves clearly show the values of the maximum response temperature (T_{max}), before which the Svalues increase, and after — they decrease. Since the presence of NH_3 in the gas mixture led to the greatest response, the effect of NH_3 on In_2O_3 films will be considered in more detail. The concentration dependences of the response of In_2O_3 films were measured at the already known values T_{max}. These dependences turned out to be linear on exposure to NH_3 (Fig. 2, *b*), and for other gases (see Table 2), the values of Sgrow up with an increase in n_g according to a exponential law. The gas sensitivity of the films In_2O_3 to NH_3 increases with measurements, under the same conditions the value S at first did not exceed 14 (Fig. 2, *a*), and at the end of the measurements was 33.3 (Fig. 2, *b*). The resistance values in the absence of target gases in the air atmosphere at T_{max} were in the interval $R = 0.1{-}2.5$ GOm.

Figure 3 shows the temperature dependences of t_{res} and t_{rec} of In_2O_3 films on exposure to CO, H_2, NH_3 and O_2. The obtained values of t_{res} and t_{rec} can only serve to evaluate the performance of In_2O_3 films under the indicated experimental conditions and include the time required to establish a steady state of the atmosphere in the measuring chamber. The sum of t_{res} and t_{rec} on exposure to target gases in the entire T range increases in the following order: $O_2 \to NH_3 \to CO \to H_2$, the smaller $t_{res} + t_{rec}$, the higher the performance. With an increase in T, there was a characteristic decrease in the values of t_{res} and t_{rec} according to an exponential law. The exception is H_2, when it is exposed to the area$T = 250{-}350$°C, there is an increase in the values of t_{res} and t_{rec}. At T_{max}, the sum of t_{res} and t_{rec} of the films In_2O_3 on exposure to CO,H_2, NH_3 and O_2 was 69.5, 68.1, 129.1, and 182 s, respectively.

Figure 4, *a* shows the time dependences of the film resistance In_2O_3 under cyclic exposure to target gases. The sections of the resistance decrease on exposure to NH_3, H_2, CO and the increase in the resistance of the films In_2O_3 after exposure to these gases are approximated by the following formulas, respectively:

$$R(t) = R_{\text{r.g.}} + A\exp(-t/\tau_1), \tag{3}$$

$$R(t) = R_{\text{air}} - B_1\exp(-t/\tau_2) - B_2\exp(-t/\tau_3) - B_3\exp(-t/\tau_4), \tag{4}$$

where t — time, A, B_1, B_2 and B_3 — constants; τ_1, τ_2, τ_3 and τ_4 — time constant. The time constant constant τ_1 is related to the relaxation time of the adsorption of the corresponding gas molecules on the surface of the semiconductor, and τ_2, τ_3 and τ_4 — to the relaxation times of the desorption of these gas molecules on the surface of the semiconductor. For the samples under study on exposure to NH_3, CO and H_2 the following conditions are fulfilled: $\tau_3 = \tau_4 \ll \tau_2$ and $\tau_2 = \tau_3 \ll \tau_4$, respectively. The sections of the resistance increase on exposure to O_2 and the resistance decrease of films In_2O_3 after its exposure are approximated by the following formulas, respectively:

$$R(t) = R_{\text{O}} - C\exp(-t/\tau_5), \tag{5}$$

$$R(t) = R_{\text{N}} + D\exp(-t/\tau_6), \tag{6}$$

where C and D — constants; τ_5 and τ_6 — time constant. The time dependences of the resistance of the In_2O_3 films can be used to determine the response drift ΔS. Quantitative assessment of ΔS values was carried out using the following

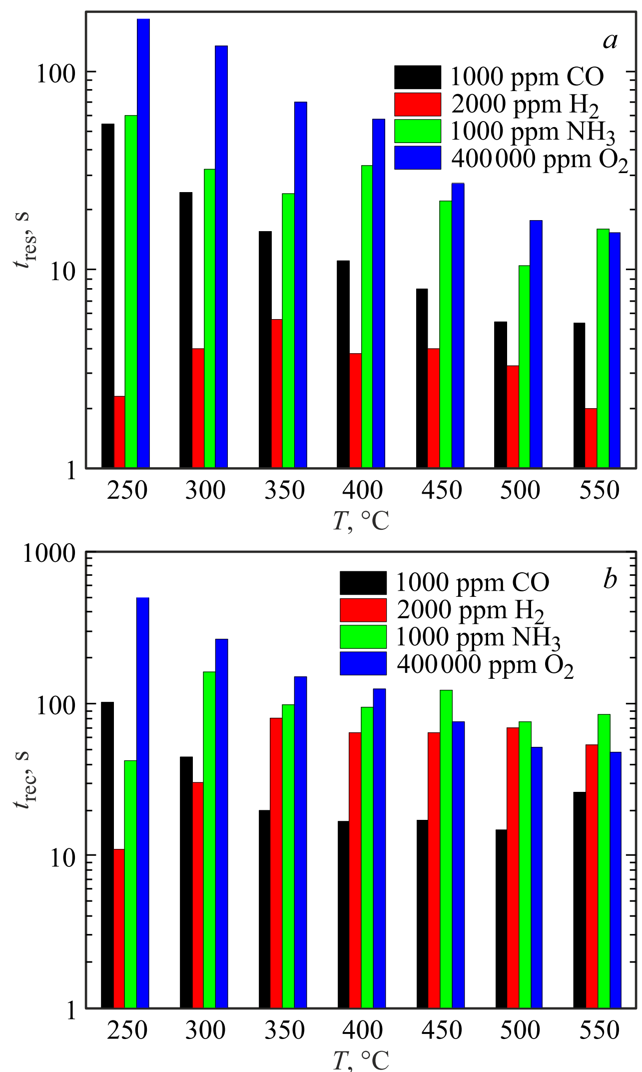

Figure 3. Temperature dependences of the response (*a*) and recovery (*b*) times of In_2O_3 films on exposure to target gases.

expression:

$$\Delta S = |(S_i/S_{av} - 1) \cdot 100|, \tag{7}$$

where S_i — response values at i-th exposure to gas; S_{av} — average response value. There were relatively high values of ΔS on exposure to CO, NH_3 and O_2, which did not exceed 12%. The greatest drift was during the first exposure to target gases, which is typical for such measurements,

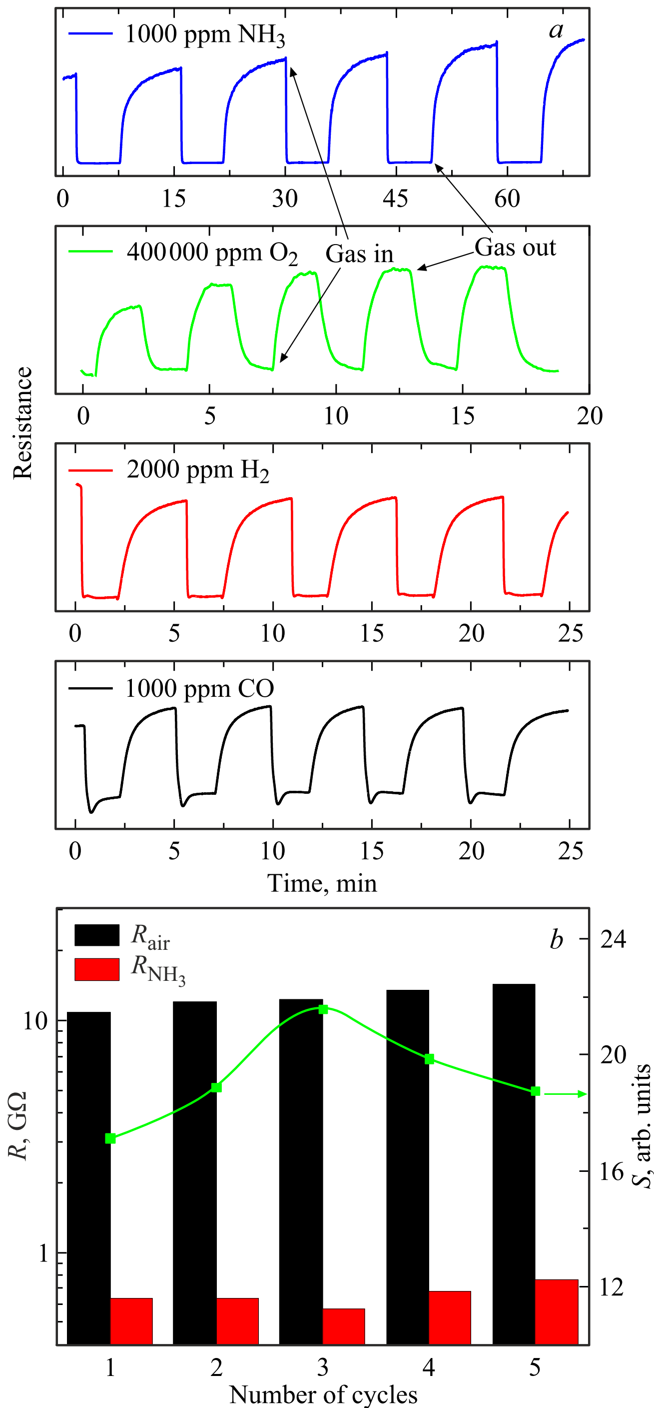

Figure 4. Time dependences of resistance under fivefold exposure to target gases (a) and dependence of R_{air}, R_{NH_3} and S on i (b) for films In_2O_3 at $T = 400°C$.

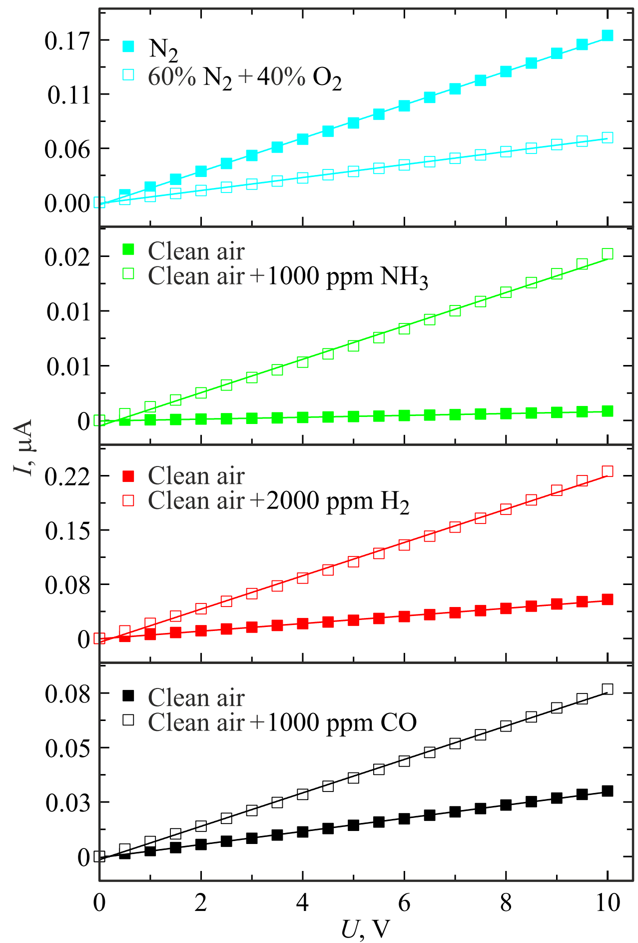

Figure 5. CVC on exposure to target gases on films In_2O_3 at T_{max}.

and an increase in the serial number i corresponds to a non-linear decrease in values ΔS. The highest repeatability under the conditions of one experiment is demonstrated by In_2O_3 films on exposure to H_2, the average value of ΔS was 0.7%. The dynamics of changes in the response of films In_2O_3 under cyclic exposure to NH_3 is shown in Fig. 4, b, where R_{NH_3} — quasi-stationary values of sample resistances in a mixture of clean dry air + 1000 ppm^{-1} NH_3.

I-V characteristics of the studied samples at T_{max} in air, N_2 and on exposure to CO, H_2, NH_3 and O_2 (Fig. 5) are linear and symmetrical. The exposure of gases resulted in a change in the CVC slope. The voltage response is almost non-existent up to $U = 10$ V. A slight decay of the response was observed only on exposure to NH_3 to $U = 2$ V, which is most likely due to the low current in an atmosphere of clean air.

3.3. Mechanism of gas sensitivity of films In_2O_3

With a known value of the electron mobility ($\mu = 60\,\text{cm}^2/(\text{V} \cdot \text{s})$ [3,5–7,17,29–31]), the temperature dependence of the electron concentration (n) and the Debye screening length (L_D) was obtained (Fig. 6). The following

Table 3. Comparison of gas sensitive characteristics of In_2O_3 with other materials when exposed to NH_3

Structure	Growth method	n_g, ppm^{-1}	T_{max}, °C	S_{max}, arb. units	Ref
Films In_2O_3	HVPE	1000 520	400	33.3 17.3	This work
Hierarchical structures In_2O_3	Powder annealing InOOH	5	300	1.9	[11]
Nanowires In_2O_3	CVD	200	25	12	[41]
Thin films In_2O_3 Thin films $In_2O_3 + CuO$	Spray pyrolysis	71	150 200	1.07 1.75	[42]
Ga_2O_3 films	Co-deposition	100	500	1.9	[38]
SnO_2 films	PEALD	1000	400	2.8	[39]
Thick films ZnO	Screen printing	1000	350	7.1	[40]
Films MoO_3	RFMS	1000	250	10	[43]
Thick films WO_3	Sol-gel	4000	450	15	[44]

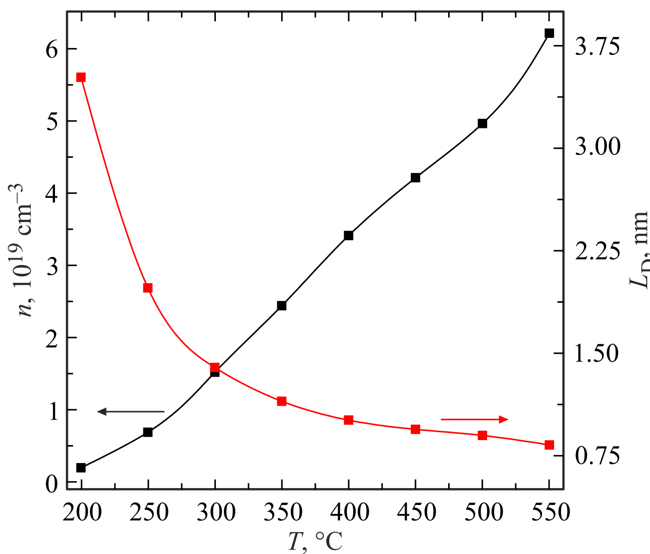

Figure 6. Temperature dependences of electron concentration and Debye screening length for films In_2O_3.

expression [32] was used to calculate the L_D values:

$$L_D = [\varepsilon_0 \varepsilon_r kT/(e^2 n)]^{0.5}, \tag{8}$$

where ε_0 — electrical constant; ε_r — static permittivity which is 10.7 for c-In_2O_3 [6,7,33]; k — Boltzmann constant; e — electron charge. According to our estimates, $L_D \ll D_g$, which indicates an over-barrier mechanism of conduction, according to which there are potential barriers for electrons at the grain interface with a height of $e\varepsilon_s$, where ε_s — is the surface potential. In the air atmosphere, molecular oxygen is chemisorbed on the surface of films In_2O_3, capturing electrons from the conduction band, which leads to the formation of an electron-poor surface layer and an increase in the upward bending of the energy bands, $e\varphi_s \propto N_i^2$, where N_i is the surface density of chemisorbed ions oxygen. The resistance in this case is described by the following expression [32]:

$$R = R_0 \exp[e\varphi_s/(kT)], \tag{9}$$

where R_0 — a parameter determined by the properties of the semiconductor, which is weakly dependent on changes in the composition of the atmosphere.

At $T > 150$°C the atomic form of chemisorbed oxygen O^- dominates on the surface of In_2O_3, which is formed as follows [34]:

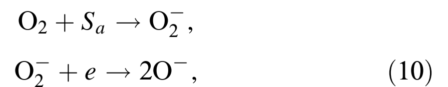

$$O_2 + S_a \rightarrow O_2^-,$$
$$O_2^- + e \rightarrow 2O^-, \tag{10}$$

where S_a — adsorption site. When O_2 is exposed to the surface of the films In_2O_3, N_i increases and, according to expression (9), R increases. The presence of reducing gases in the gas mixture leads to a decrease in N_i as a result of their interaction with O^- on the surface of In_2O_3 films. The interaction of reducing gases with O^- on the surface of In_2O_3 films can be described by the following chemical equations [21,35–37]:

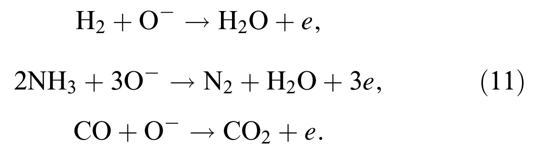

$$H_2 + O^- \rightarrow H_2O + e,$$
$$2NH_3 + 3O^- \rightarrow N_2 + H_2O + 3e, \tag{11}$$
$$CO + O^- \rightarrow CO_2 + e.$$

As a result of these reactions, the surface density of chemisorbed oxygen ions N_i, the value of $e\varphi_s$ and the width of the space charge area decrease, electrons enter the conduction band of the In_2O_3 films, and the reaction products are desorbed from the surface in the form of molecules H_2O, N_2 and CO_2.

3.4. Comparison of gas sensitivity to NH_3 structures based on In_2O_3 with other MOS

Films In_2O_3, obtained by the HVPE method show a very high sensitivity to NH_3. The values of T_{max} and the corresponding values of the maximum response (S_{max}) at fixed n_g

are presented and compared with other papers [11,38–44] in Table 3. The most interesting results were shown by NH_3sensors based on In_2O_3 [11,41,42]. Despite the not so high sensitivity, the S values turned out to be relatively high at significantly lower n_g and T_{max}, which is probably due to structural features that lead to high sensitivity, but significantly limit the performance [35,45,46]. Films based on other MOS are characterized by a significantly lower sensitivity than In_2O_3 under fairly similar measurement conditions. The response values obtained at the minimum studied gas concentration are still quite high, which is of interest for further studies at lower n_g. The results presented in Table 3 indicate the prospect of using In_2O_3 for detecting NH_3 and the opportunity of using the HVPE method to create structures with high gas sensitivity based on this material.

4. Conclusion

The gas-sensitive characteristics of In_2O_3 films $0.5\,\mu$m thick, obtained by the HVPE method, are studied on exposure to H_2, NH_3, O_2 and CO in a wide temperature range. Sensitivity to gases begins to be shown at temperatures of $> 200^\circ$C. The highest performance and response are characteristic on exposure to H_2, CO and NH_3, respectively. Films In_2O_3 were highly stable under repeated exposure to gases, and there was the smallest drift for H_2. There was the highest gas sensitivity on exposure to NH_3. The maximum response was obtained at a temperature of 400°C and amounted to 33.3 on exposure to $1000\,\text{ppm}^{-1}$ NH_3, and the response and recovery times did not exceed 34 and 96 s. The results obtained were compared with other works, the comparison showed the possibility of using this material as gas sensors NH_3. A qualitative mechanism of gas sensitivity is proposed. It is shown that the interaction of gases with chemisorbed oxygen on the surface of In_2O_3 films leads to a change in the height of the potential barrier at the grain boundary.

Acknowledgments

The for Collective Use „Nanotech“ Institute of Strength Physics and Materials Science of Siberian Branch of RAS for providing FESEM images.

Funding

The study was supported by the Russian Science Foundation (grant No. 20-79-10043).

Conflict of interest

The authors declare that they have no conflict of interest.

References

[1] B. Lu, P. Chen, J. Zou, B. Yao, H. Chen. Phys. Status Solidi A, **215** (21) 1800401 (2018).
[2] G. Domenech-Gila, J. Samaa, P. Pellegrinoa, S. Barthb, I. Graciac, C. Canec, A. Romano-Rodrigueza. Sensors Actuators B: Chem., **238**, 447 (2016).
[3] J.A. Spencer, A.L. Mock, A.G. Jacobs, M. Schubert, Y. Zhang, M.J. Tadjer. Appl. Phys. Rev., **9** (1), 011315 (2022).
[4] S.H. Babu, S. Kaleemulla, N.M. Rao, C. Krishnamoorthi. J. Magn. Magn. Mater., **416**, 66 (2016).
[5] P.D.C. King, T.D. Veal, F. Fuchs, Ch.Y. Wang, D.J. Payne, A. Bourlange, H. Zhang, G.R. Bell, V. Cimalla, O. Ambacher, R.G. Egdell, F. Bechstedt, C.F. McConville. Phys. Rev. B, **79**, 205211 (2009).
[6] M. Stokey, R. Korlacki, S. Knight, A. Ruder, M. Hilfiker, Z. Galazka, K. Irmscher, Y. Zhang, H. Zhao, V. Darakchieva, M. Schubert. J. Appl. Phys., **129**, 225102 (2021).
[7] K.H.L. Zhang, V.K. Lazarov, T.D. Veal, F.E. Oropeza, C.F. McConville, R.G. Egdell, A. Walsh. J. Phys.: Condens. Matter, **23**, 334211 (2011).
[8] A. Walsh, D.O. Scanlon. Phys. Rev. B, **88**, 161201 (2013).
[9] T. de Boer, M.F. Bekheet, A. Gurlo, R. Riedel, A. Moewes. Phys. Rev. B, **93**, 155205 (2016).
[10] V. Golovanova, M.A. Maki-Jaskari, T.T. Rantalab, G. Korotcenkovc, V. Brinzaric, A. Cornetd, J. Moranted. Sensors Actuators B: Chem., **106** (2), 563 (2005).
[11] H. Jiang, L. Zhao, L. Gai, L. Ma, Y. Maa, M. Lib. CrystEngComm., (**35**), 7003 (2013).
[12] A. Gurlo, R. Riedel. IEEE Sensors, **4**, 1505 (2008).
[13] L. Gao, F. Ren, Z. Cheng, Y. Zhang, Q. Xiangc, J. Xu. CrystEngComm., (**17**), 3268 (2015).
[14] N. Sui, S. Cao, P. Zhang, T. Zhou, T. Zhang. J. Hazardous Mater., **418**, 126290 (2021).
[15] L. Song, K. Dou, R. Wang, P. Leng, L. Luo, Y. Xi, C.C. Kaun, N. Han, F. Wang, Y. Chen. ACS Appl. Mater. & Interfaces, **12** (1), 1270 (2019).
[16] F. Chen, M. Yang, X. Wang, Y. Song, L. Guo, N. Xie, X.Kou, X. Xu, Y. Sun, G. Lu. Sensors Actuators B: Chem., **290**, 459 (2019).
[17] R. Togashi, S. Numata, M. Hayashida, T. Suga, K. Goto, A. Kuramata, S. Yamakoshi, P. Paskov, B. Monemar, Y. Kumagai. Jpn. J. Appl. Phys., **55** (12), 1202B3 (2016).
[18] H. Nakahata, R. Togashi, K. Goto, B. Monemar, Y. Kumagai. J. Cryst. Growth, **563**, 126111 (2021).
[19] S.I. Stepanov, V.I. Nikolaev, A.I. Pechnikov, M.P. Scheglov, A.V. Chikiryaka, A.V. Chernykh, M.A. Odnobludov, V.D. Andreeva, A.Y. Polyakov. Phys. Status Solidi A, **218** (3), 2000442 (2020).
[20] V.I. Nikolaev, A.V. Almaev, B.O. Kushnarev, A.I. Pechnikov, S.I. Stepanov, A.V. Chikiryaka, R.B. Timashov, M P. Shcheglov, P.N. Butenko, E.V. Chernikov. Pis'ma ZhTF, **48** (14), 37 (2022) (in Russian).
[21] N.N. Yakovlev, A.V. Almaev, V.I. Nikolaev, B.O. Kushnarev, A.I. Pechnikov, S.I. Stepanov, A.V. Chikiryaka, R.B. Timashov, M.P. Scheglov, P.N. Butenko, D.A. Almaev, E.V. Chernikov. Materials Today Commun., **34**, 105241 (2023).
[22] X. Hou, Y. Zou, M. Ding, Y. Qin, Z. Zhang, X. Ma, P. Tan, S. Yu, X. Zhou, X. Zhao, G. Xu, H. Sun, S. Long. J. Phys. D: Appl. Phys., **54**, 043001 (2020).

[23] S.J. Pearton, Jiancheng Yang, Patrick H. Cary, F. Ren, Jihyun Kim, Marko J. Tadjer, Michael A. Mastro. Appl. Phys. Rev., **5** (1), 011301 (2018).
[24] D. Kaur, M. Kumar. Adv. Optical Mater, **9** (9), 2002160 (2021).
[25] A.V. Almaev, V.I. Nikolaev, N.N. Yakovlev, P.N. Butenko, S.I. Stepanov, A.I. Pechnikov, M.P. Scheglov, E.V. Chernikov. Sensors Actuators B: Chem., **364**, 131904 (2022).
[26] A.V. Almaev, V.I. Nikolaev, P.N. Butenko, S.I. Stepanov, A.I. Pechnikov, N.N. Yakovlev, I.M. Sinyugin, S.V. Shapenkov, M.P. Scheglov. Phys. Status Solidi B, **259** (2), 2100306 (2021).
[27] A.V. Almaev, V.I. Nikolaev, S.I. Stepanov, A.I. Pechnikov, A.V. Chikiryaka, N.N. Yakovlev, V.M. Kalygina, V.V. Kopyev, E.V. Chernikov. J. Phys. D: Appl. Phys., **53** (41), 414004 (2020).
[28] N.N. Yakovlev, V.I. Nikolaev, S.I. Stepanov, A.V. Almaev, A.I. Pechnikov, E.V. Chernikov, B.O. Kushnarev. IEEE Sensors J., **21** (13), 8 (2021).
[29] Z. Galazka, R. Uecker, R. Fornari. J. Cryst. Growth, **388**, 61 (2014).
[30] H. Kostlin, R. Jost, W. Lems. Phys. Status Solidi A, **29** (1), 87 (1975).
[31] P. Thilakan, J. Kumar. Thin Sol. Films, **292** (1−2), 50 (1997).
[32] V.I. Gaman. *Fizika poluprovodnikovykh gazovykh sensorov* (Tomsk, Izd-vo NTL, 2012). (in Russian).
[33] A. Walsh, C.R.A. Catlow, A.A. Sokol, S.M. Woodley. Chem. Mater., **21**, 4962 (2009).
[34] K.K. Makhija, A. Ray, R.M. Patel, U.B. Trivedi, H.N. Kapse. Bull. Mater. Sci., **28** (1), 9 (2005).
[35] H. Kim, C. Jin, S. An, C. Lee. Ceramics International, **38** (5), 3563 (2012).
[36] N. Yamazoe, K. Shimanoe. J. Sensors, **21** (2009).
[37] V.I. Gaman. Russian Phys. J., **51** (4), 425 (2008).
[38] N. Vorobyeva, M. Rumyantseva, V. Platonov, D. Filatova, A. Chizhov, A. Marikutsa, I. Bozhev, A. Gaskov. Nanomaterials, **11** (11), 2938 (2021).
[39] D.H. Kim, W-S. Kim, S.B. Lee, S-H. Hong. Sensors Actuators B: Chem., **147** (2), 653 (2010).
[40] M.S. Wagh, G.H. Jain, D.R. Patil, S.A. Patil, L.A. Patil. Sensors Actuators B: Chem., **115** (1), 128 (2006).
[41] C. Li, D. Zhang, B. Lei, S. Han, X. Lie, C. Zhou. J. Phys. Chem., **107** (45), 12451 (2003).
[42] A.A. Hameed, S. Hamid, A.L. Jumaili. Iraqi J. Sci., **62** (7), 2204 (2021).
[43] W-C. Chang, X. Qi, J-C. Kuo, S.L. Lee, S-K. Ng, D. Chen. CrystEngComm., (16), 5125 (2011).
[44] V. Srivastava, K. Jain. Sensors Actuators B: Chem., **133** (1), 46 (2008).
[45] Z. Liu, T. Yamazaki, Y. Shen, T. Kikuta, N. Nakatani, Y. Li. Sensors Actuators B: Chem., **129** (2), 666 (2008).
[46] N.D. Cuong, Y.W. Park, S.G. Yoon. Sensors Actuators B: Chem., **140** (1), 240 (2009).

Translated by E.Potapova